

Closed-loop Control Design and Motor Allocation for a Lower-limb Cable-driven Exoskeleton: A Switched Systems Approach

Chen-Hao Chang¹, Jonathan Casas¹, Victor H. Duenas¹

Abstract—Powered lower-limb exoskeletons provide assistive torques to coordinate limb motion during walking in individuals with movement disorders. Advances in sensing and actuation have improved the wearability and portability of state-of-the-art exoskeletons for walking. Cable-driven exoskeletons offload the actuators away from the user, thus rendering light-weight devices to facilitate locomotion training. However, cable-driven mechanisms experience a slacking behavior if tension is not accurately controlled. Moreover, counteracting forces can arise between the agonist and antagonist motors yielding undesired joint motion. In this paper, the strategy is to develop two control layers to improve the performance of a cable-driven exoskeleton. First, a joint tracking controller is designed using a high-gain robust approach to track desired knee and hip trajectories. Second, a motor synchronization objective is developed to mitigate the effects of cable slacking for a pair of electric motors that actuate each joint. A sliding-mode robust controller is designed for the motor synchronization objective. A Lyapunov-based stability analysis is developed to guarantee a uniformly ultimately bounded result for joint tracking and exponential tracking for the motor synchronization objective. Moreover, an average dwell time analysis provides a bound on the number of motor switches when allocating the control between motors that actuate each joint. An experimental result with an able-bodied individual illustrates the feasibility of the developed control methods.

Index Terms—Cable-driven exoskeleton, nonlinear control

I. INTRODUCTION

Regaining mobility is a top priority for individuals with movement disorders, whose locomotion is affected by muscle weakness and reduced leg coordination. Powered lower-limb exoskeletons aim to restore and improve function of people with spinal cord injury and post-stroke. Powered exoskeletons vary in their design, wearability, sensing, and actuation. Existing powered exoskeletons use electrical motors [1], hydraulic [2] and pneumatic actuators [3], [4]. The actuators used to outfit the exoskeleton influence the magnitude and response of the inputs applied to the body and thus the human-robot interaction. Particularly, traditional exoskeletons use frames to affix actuators to the human body, however this approach results in increased system's inertia and metabolic costs of walking [5]. Therefore, the design of portable and lighter exoskeleton devices has been the focus of recent research to achieve transparent motion and enable human volition [6].

Cable-driven transmission mechanisms offload actuators away from the human to reduce the weight imposed on the body and thus reduces the burden on the user-side.

Such mechanisms have been widely applied for orthotic devices (e.g., lower-limb [7], [8], upper-limb [9], [10], hand orthoses [11]) to provide torques about the joints to assist or augment human function. Since cables cannot transmit compression forces, at least $l + 1$ cables are required to control l DOFs to provide an agonist-antagonist movement [12]. Despite the benefits of cable-driven mechanisms, two critical issues arise: (1) cables experience a slack behavior if the tension is not accurately controlled, thus affecting the response time; (2) undesired agonist-antagonist coordination may produce counteracting torques about a joint. Hence, it is essential to develop effective control strategies to ensure coordinated or synchronized motion in a multi-joint system.

Multiple strategies have been developed to mitigate the undesirable slacking behavior and coordination issues in cable-driven systems. A mechanical approach with closed pulley transmission (one motor with two cables) was used in [13] to achieve bi-directional joint movement. Alternatively, a motor synchronization approach was developed in [7], where one motor controlled the joint torque, and its antagonist motor was synchronized using a closed-loop proportional controller. The control designs in [14], [15] combined the robot and actuator dynamics and provided proofs of stability. In this paper, the strategy is to develop controllers for a cable-driven exoskeleton by segregating the control into layers: the motor layer to mitigate the slacking behavior in cables that actuate joints, and the joint layer to achieve the tracking objective. This layered approach is developed to improve the scalability and prototyping of gait controllers.

In a typical multi-layer control system, the higher layer usually generates the gait pattern to be tracked [16] or force fields [17]. The lower layer focuses on allocating control among actuators and generate control inputs. In this paper, the control allocation is addressed using switching control, which requires a switched-based stability analysis. Up to the best knowledge of the authors, the existing literature on cable-driven exoskeletons has not exploited switched systems control and analysis to improve tracking performance. Particularly, an average dwell time analysis as in [18] is introduced to bound the number of switches (i.e., control allocation switches) within a time period to prevent counteracting forces from being applied about a joint by a pair of electric motors.

In this paper, the control design to actuate leg joints using cable-driven mechanisms is segregated into layers. First, the joint control layer generates the control input to track the desired joint trajectory. A high-gain robust kinematic tracking controller is designed for the hip and knee joints. Second,

¹Department of Mechanical and Aerospace Engineering, Syracuse University, Syracuse NY 13244, USA. Email: {cchang21, jacasasb, vhduenas}@syr.edu

the motor control layer includes a pair of electric motors to provide bidirectional motion about a joint. For any joint actuated by a pair of electric motors, the motor that provides cable tension to actuate the joint is called the lead motor. The other motor is called the follower motor. Therefore, the lead motor receives the joint kinematic control input to actuate the joint in the desired direction (e.g., joint flexion). Meanwhile, a closed-loop robust sliding-based controller is developed for the follower motor to ensure synchronization with the lead motor (i.e., mitigate the potential slacking behavior when not actuating the joint). Once the desired joint direction reverses (e.g., joint extension), the previous lead motor becomes the follower motor, and vice versa. A Lyapunov-based stability analysis is provided to guarantee uniformly ultimately bounded result for joint tracking and exponential tracking for the motor synchronization objective (i.e., prevent cable slacking). An average dwell time analysis provides a bound on the number of motor switches when allocating the control between motors that actuate each joint. An experimental result with an able-bodied individual is presented to illustrate the performance of developed controllers.

II. HUMAN-EXOSKELETON DYNAMIC MODEL

A motorized exoskeleton with a user can be modeled as a four-link bipedal walking system in the sagittal plane as follows

$$M(q)\ddot{q} + C(q, \dot{q})\dot{q} + G(q) + P(q, \dot{q}) + d(t) = \tau_e(q, \dot{q}, t), \quad (1)$$

where $q : \mathbb{R}_{\geq t_0} \rightarrow \mathbb{R}^4$ denotes the measurable hip and knee joint angles on both sides, $\dot{q}, \ddot{q} : \mathbb{R}_{\geq t_0} \rightarrow \mathbb{R}^4$ denote the measurable joint angular velocities and unmeasurable joint angular accelerations, respectively, where $t_0 \in \mathbb{R}_{>0}$ is denoted as initial time; $M : \mathbb{R}^4 \rightarrow \mathbb{R}_{>0}^{4 \times 4}$ denotes the combined human-exoskeleton inertia; $C : \mathbb{R}^4 \times \mathbb{R}^4 \rightarrow \mathbb{R}^{4 \times 4}$ and $G : \mathbb{R}^4 \rightarrow \mathbb{R}^4$ denote centripetal-Coriolis and gravitational effects, respectively; $P : \mathbb{R}^4 \times \mathbb{R}^4 \rightarrow \mathbb{R}^4$ denotes the damping and viscoelastic effects; and $d : \mathbb{R}_{\geq t_0} \rightarrow \mathbb{R}^4$ denotes unmodeled terms and disturbances. The torque produced by the electrical motors are expressed as $\tau_e : \mathbb{R}^4 \times \mathbb{R}^4 \times \mathbb{R}_{\geq t_0} \rightarrow \mathbb{R}^4$. A body-weight support system is utilized to support and stabilize the trunk (i.e., trunk dynamics are not considered).

A. Cable-driven Actuator System

The lower-limb exoskeleton is actuated by electric motors utilizing customized cable-driven mechanisms. Electric motors can be segregated into extension (ex) and flexion (fl) actuator groups with respect to each joint. Forces are transmitted to each joint via Bowden cables. A pair of motors control extension and flexion for each joint. Four pairs of motors are used to control bilaterally the hip and knee joints. One of the motors in a pair, called the lead motor, receives the control input of the joint tracking controller to achieve the desired motion (e.g., flexion or extension). The second motor in a pair, called the follower motor, rotates in the opposite direction to the lead motor. The follower motor receives the input of a synchronization controller, which prevents force

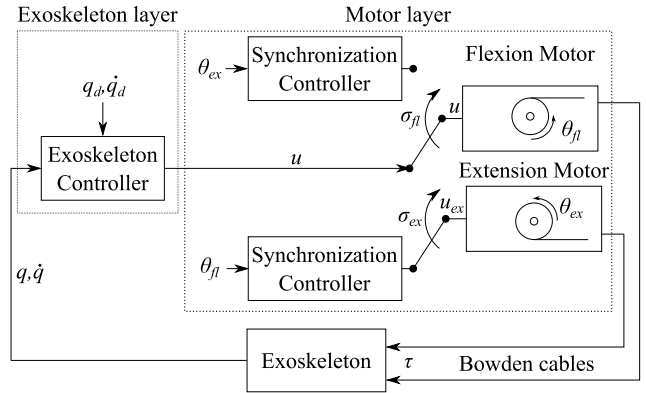


Fig. 1. Schematic representation for the multi-layer control system (illustrated for flexion motion). The joint control layer sends a flexion control input ($u > 0$) to the motor control layer. The switching signal is triggered as $\sigma_{fl} = 1$ to allocate the control input to the flexion motor. The extension motor (follower motor in this case, i.e., $\sigma_{ex} = 0$) is allocated to follow the angle of the flexion motor (lead motor) commanded by the motor synchronization controller (u_{ex}).

tension conflicts with the lead motor, mitigate cable slack, and provides fast force response.

The torque produced by the motors to actuate the exoskeleton is defined as

$$\tau_e(q, \dot{q}, t) \triangleq B_\sigma(q, \dot{q})u(t), \quad (2)$$

$$B_\sigma(q, \dot{q}) \triangleq \sum_{n=1}^8 B_n \sigma_n(t), \quad (3)$$

where the subscript $n \in \{1, 2, \dots, 8\} \subset \mathbb{N}$ denotes the motor index, and let \mathcal{E}, \mathcal{F} the set of all extension and flexion motors, respectively. The control input $u : \mathbb{R}_{\geq t_0} \rightarrow \mathbb{R}^4$ is designed in Section III, where positive and negative control inputs refer to flexion and extension movements, respectively. The unknown individual motor control effectiveness is denoted as $B_n : \mathbb{R}_{>0}^{4 \times 4}, \forall n \in \mathcal{E} \cup \mathcal{F}$. A piecewise constant switching signal for each motor $\sigma_n(t) \in \{0, 1\}$ determines if the motor is applying exoskeleton control input. The subscript $\sigma \in \mathcal{S}$, such that $\mathcal{S} = \{1, 2, 3, \dots, i\}$ denotes the i^{th} possible lead motors combination. The lumped switched motor control effectiveness is denoted as B_σ . A schematic representation of the time-varying control system is presented in Figure 1. The following properties are exploited in the subsequent control design and stability analysis.

Property 1. $c_m \|\xi\|^2 \leq \xi^T M(q)\xi \leq c_M \|\xi\|^2, \forall \xi \in \mathbb{R}^4$, where c_m and c_M are known positive constants.

Property 2. $\|C(q, \dot{q})\| \leq c_c \|\dot{q}\|$, where c_c is a known positive constant.

Property 3. $\|G(q)\| \leq c_g$, where c_g is a known positive constant.

Property 4. $\|P(q, \dot{q})\| \leq c_{p1} + c_{p2} \|\dot{q}\|$, where c_{p1} and c_{p2} are known positive constants.

Property 5. $\|d(t)\| \leq d_{exo}$, where d_{exo} is a known positive constant.

Property 6. $\underline{B} \|\xi\|^2 \leq \xi^T B_\sigma \xi \leq \overline{B} \|\xi\|^2, \forall \xi \in \mathbb{R}^4, \forall \sigma \in \mathcal{S}$, where \underline{B} and \overline{B} are known positive constants.

Property 7. The skew-symmetry $\xi^T \left(\frac{1}{2} \dot{M} - C \right) \xi = 0, \forall \xi \in \mathbb{R}^4$ [19].

B. Follower Motor Model

Each motor system in the exoskeleton includes an electric motor, a gearbox and a pulley. The motor system dynamics are modeled to develop the motor synchronization controller as follows [19]

$$J_n \ddot{\theta}_n + D_n \dot{\theta}_n + d_n(t) = B_n u_n \bar{\sigma}_n(t), \quad (4)$$

where $\theta_n, \dot{\theta}_n, \ddot{\theta}_n$ denotes measurable motor's angle, angular velocity, and unmeasurable angular acceleration of the n^{th} motor system. The inertia $J_n \in \mathbb{R}_{>0}$, damping constant $D_n \in \mathbb{R}$, and disturbances with friction and any unmodeled terms $d_n \in \mathbb{R}$. The control input $u_n \in \mathbb{R}$ corresponding to the n^{th} motor is designed in Section III. A piecewise constant switching signal $\bar{\sigma}_n$ that determines if the motor is applying motor synchronization control input. The switching signals σ_n and $\bar{\sigma}_n$ are opposite to each other, i.e., if the n^{th} motor at time t is performing motor synchronization, then $\bar{\sigma}_n(t) = 1, \sigma_n(t) = 0$, and vice versa. The following properties are exploited in the subsequent control design and stability analysis.

Property 8. $J_n, D_n, d_n(t)$ satisfy the inequalities $c_j \leq J_n \leq c_J, c_d \leq D_n \leq c_D, c_{de} \leq d_n(t) \leq c_{De}, \forall n \in \mathcal{E} \cup \mathcal{F}$, where $c_j, c_J, c_d, c_D, c_{de}$, and c_{De} are known positive constants.

Property 9. $\underline{B}_n \|\xi\|^2 \leq \xi^T B_n \xi \leq \overline{B}_n \|\xi\|^2, \forall \xi \in \mathbb{R}^4, \forall n \in \mathcal{E} \cup \mathcal{F}$, where \underline{B}_n and \overline{B}_n are known positive constants.

III. CONTROL DEVELOPMENT

The control objectives of this paper are twofold. First, a high-gain tracking controller is developed to track desired hip and knee joint angles. Second, a robust sliding-mode controller is developed to achieve the synchronization objective for the follower motor.

A. Joint Kinematic Control

The measurable joint position trajectory tracking error $\xi : \mathbb{R}_{\geq t_0} \rightarrow \mathbb{R}^4$ and filtered tracking error $\eta : \mathbb{R}_{\geq t_0} \rightarrow \mathbb{R}^4$ are defined as

$$\xi(t) \triangleq q_d(t) - q(t), \quad (5)$$

$$\eta(t) \triangleq \dot{\xi}(t) + \alpha \xi(t), \quad (6)$$

where $\alpha \in \mathbb{R}$ is a selectable positive control gain and $q_d(t), \dot{q}_d(t), \ddot{q}_d(t) : \mathbb{R}_{\geq t_0} \rightarrow \mathbb{R}^4$ are bounded desired trajectories. The open-loop error system is obtained by taking the time derivative of (6), pre-multiplying M , substituting (5), and performing algebraic manipulation as

$$M \dot{\eta} = \chi - C \eta - B_\sigma u - \xi, \quad (7)$$

where the auxiliary signal $\chi : \mathbb{R}_{\geq t_0} \rightarrow \mathbb{R}^4$ is defined as

$$\chi \triangleq M \left(\ddot{q}_d + \alpha \dot{\xi} \right) + C \left(\dot{q}_d + \alpha \xi \right) + G + P + d. \quad (8)$$

Using Properties 1-5, the auxiliary signal can be upper bounded as

$$\|\chi\| \leq \rho (\|z_1\|), \quad (9)$$

where $z_1 \triangleq \begin{bmatrix} \xi^T & \eta^T \end{bmatrix}^T : \mathbb{R}_{\geq t_0} \rightarrow \mathbb{R}^8, \rho (\|z_1\|) \triangleq \rho_1 + \rho_2 \|z_1\| + \rho_3 \|z_1\|^2$, and $\rho_1, \rho_2, \rho_3 \in \mathbb{R}_{\geq 0}$. The controller is designed as

$$u = k_1 \eta + \frac{1}{\epsilon} \rho^2 (\|z_1\|) \eta, \quad (10)$$

where $k_1, \epsilon \in \mathbb{R}_{>0}$ are positive selectable gains. The closed-loop error system can be obtained by substituting (10) into (7) as

$$M \dot{\eta} = \chi - C \eta - \xi - B_\sigma \left(k_1 \eta + \frac{1}{\epsilon} \rho^2 (\|z_1\|) \eta \right). \quad (11)$$

B. Motor Synchronization Control

Let $\varrho = \{ex, fl\}$ denote the pair of motors acting on a joint, where, ex and fl stand for the extension and flexion motors, respectively. The measurable position tracking error $e : \mathbb{R}_{\geq t_0} \rightarrow \mathbb{R}$ and filtered tracking error $r : \mathbb{R}_{\geq t_0} \rightarrow \mathbb{R}$ are defined as

$$e(t) \triangleq \theta_{fl}(t) - \theta_{ex}(t), \quad (12)$$

$$r(t) \triangleq \dot{e}(t) + \beta e(t), \quad (13)$$

where $\beta \in \mathbb{R}_{>0}$ is a selectable positive control gain. The angles for flexion and extension motor are denoted as $\theta_{fl}(t)$ and $\theta_{ex}(t)$, respectively. The controllers for extension and flexion motor can be designed separately as follows.

1) *Extension motor (ex):* The synchronization control for the extension motor is designed to track the flexion motor angle θ_{fl} . Taking derivative of the filtered tracking error (13), pre-multiplying by J_{ex} , substituting (12), and then performing algebraic manipulation yields

$$J_{ex} \dot{r} = \chi_{ex} - B_{ex} u_{ex} - e, \quad (14)$$

where the auxiliary signal $\chi_{ex} : \mathbb{R} \times \mathbb{R}_{\geq t_0} \rightarrow \mathbb{R}$ is defined as

$$\chi_{ex} = J_{ex} \left(\ddot{\theta}_{fl} + \beta \dot{e} \right) + D_{ex} \left(\dot{\theta}_{fl} - \dot{e} \right) + d_{ex} + e. \quad (15)$$

Based on (14) and the stability analysis in Section IV, the controller is designed as

$$u_{ex} = k_2 r + (k_3 + k_4 \|z_2\|) \text{sgn}(r), \quad (16)$$

where $z_2 \triangleq \begin{bmatrix} e & r \end{bmatrix}^T : \mathbb{R}_{\geq t_0} \rightarrow \mathbb{R}^2$, and $k_2, k_3, k_4 \in \mathbb{R}_{>0}$ are positive selectable gains.

2) *Flexion motor (fl):* The synchronization control objective for the flexion motor is to track the extension motor angle θ_{ex} . Utilizing a similar process as for the control development of the extension motor yields

$$J_{fl} \dot{r} = \chi_{fl} + B_{fl} u_{fl} - e, \quad (17)$$

where the auxiliary signal $\chi_{fl} : \mathbb{R} \times \mathbb{R}_{\geq t_0} \rightarrow \mathbb{R}$ is defined as

$$\chi_{fl} = -J_{fl} \left(\ddot{\theta}_{ex} - \beta \dot{e} \right) - D_{fl} \left(\dot{\theta}_{ex} - \dot{e} \right) - d_{fl} + e. \quad (18)$$

Based on (17) and the stability analysis in Section IV, the controller can be designed as

$$u_{fl} = -k_2 r - (k_3 + k_4 \|z_2\|) \operatorname{sgn}(r). \quad (19)$$

Given the open-loop dynamics in (14), (17) and control design in (16), (19), the closed-loop error dynamics can be compactly expressed as

$$J_\varrho \dot{r} = \chi_\varrho - e - B_\varrho (k_2 r + (k_3 + k_4 \|z_2\|) \operatorname{sgn}(r)). \quad (20)$$

Similarly, after leveraging the Property 8, the auxiliary signals in (15) and (18) can be upper bounded as

$$\|\chi_\varrho\| \leq c_1 + c_2 \|z_2\|, \quad (21)$$

where $c_1, c_2 \in \mathbb{R}_{>0}$ are positive bounding constants. From Theorem 1, the lead motor's control input u , joint angle, angular velocity, and acceleration are bounded, which implies that the desired synchronization trajectories θ_{fl} for the extension motor and θ_{ex} for the flexion motor are bounded.

IV. STABILITY ANALYSIS

The following theorems examine the stability for the developed joint tracking and motor synchronization controllers. Theorem 1 demonstrates global uniformly ultimately bounded (GUUB) for the joint tracking errors. Theorem 2 shows exponential tracking of motor synchronization errors across multiple switching time period. Theorem 3 uses an average dwell time analysis to provide a bound on the number of motor switches and ensures exponential tracking under fast switching.

Theorem 1. *Given the closed-loop error system in (11), the controller in (10) ensures globally uniformly ultimately bounded (GUUB) in the sense that*

$$V \leq V(0)e^{-\delta t} + \frac{\epsilon}{\delta} (1 - e^{-\delta t}), \quad (22)$$

where $\delta = \frac{1}{b} \min\{\alpha, \underline{B}k_1\}$.

Proof. Defining a nonnegative, continuously differentiable Lyapunov function $V : \mathbb{R}^4 \times \mathbb{R}^4 \times \mathbb{R}_{\geq t_0} \rightarrow \mathbb{R}$ as

$$V = \frac{1}{2} \xi^T \xi + \frac{1}{2} M \eta^T \eta, \quad (23)$$

which satisfies the following inequalities

$$a \|z_1\|^2 \leq V(z_1, t) \leq b \|z_1\|^2, \quad (24)$$

where $a = \min(\frac{1}{2}, \frac{1}{2}c_m)$, $b = \max(\frac{1}{2}, \frac{1}{2}c_M)$ are positive known constants. After substituting for (11) and canceling common terms, the time derivative of (23) can be expressed as

$$\begin{aligned} \dot{V} = & -\alpha \xi^T \xi + \frac{1}{2} \dot{M} \eta^T \eta + \eta^T \left[\chi - C \eta \right. \\ & \left. - B_\sigma \left(k_1 \eta + \frac{1}{\epsilon} \rho^2 (\|z_1\|) \eta \right) \right]. \end{aligned} \quad (25)$$

With the condition in (9), Property (6) and Property (7), (25) can be upper bounded as

$$\dot{V} \leq -\alpha \xi^T \xi - \underline{B}k_1 \eta^T \eta + \eta^T |\rho| \left[1 - \frac{\underline{B}|\eta| |\rho|}{\epsilon} \right]. \quad (26)$$

The inequality can be further upper bounded as

$$\dot{V} \leq -\alpha \xi^T \xi - \underline{B}k_1 \eta^T \eta + \epsilon, \quad (27)$$

$$\leq -\delta V + \epsilon. \quad (28)$$

Based on (24) and (28), the GUUB result in (22) can be obtained. Since $V \in \mathcal{L}_\infty$, $\xi, \eta \in \mathcal{L}_\infty$ (i.e., $z_1 \in \mathcal{L}_\infty$), which implies that $u \in \mathcal{L}_\infty$ in (10) and $q, \dot{q} \in \mathcal{L}_\infty$. Furthermore, $\ddot{q} \in \mathcal{L}_\infty$. ■

Theorem 2. *Given the closed-loop error system in (20), the controller in (16) and (19) ensures exponential tracking in the sense that*

$$\|z_2(t)\| \leq \sqrt{\frac{b_\varrho}{a_\varrho}} \exp\left(-\frac{\lambda_\varrho}{2}(t-t_\omega)\right) \|z_2(t_\omega)\|, \quad (29)$$

$\forall t \in (0, \infty), \forall \omega$, where ω represents the ω^{th} time the system is activated and $\lambda_\varrho = \frac{1}{b_\varrho} \min\{\beta, \underline{B}_n k_2\}$, provided the following sufficient gain conditions are satisfied

$$k_3 \geq \frac{c_1}{\underline{B}_n}, k_4 \geq \frac{c_2}{\underline{B}_n}. \quad (30)$$

Proof. Defining a nonnegative, continuously differentiable Lyapunov function for the pair motor system $V_\varrho : \mathbb{R} \times \mathbb{R} \times \mathbb{R}_{\geq t_0} \rightarrow \mathbb{R}$ as

$$V_\varrho = \frac{1}{2} e^2 + \frac{1}{2} J_\varrho r^2, \quad (31)$$

which satisfies the following inequalities

$$a_\varrho \|z_2\|^2 \leq V_\varrho(z_2, t) \leq b_\varrho \|z_2\|^2, \quad (32)$$

where $a_\varrho = \min(\frac{1}{2}, \frac{1}{2}c_j)$, $b_\varrho = \max(\frac{1}{2}, \frac{1}{2}c_J)$ are positive known constants. Since there exist discontinuous terms in motor synchronization control input (16) and (19), the Filippov method is used to analyze the system's stability. Let $z_2(t)$ be a Filippov solution to the differential inclusion $\dot{z}_2 \in K[h](z_2)$, where $K[\cdot]$ is defined as in [20] and h is defined by using (20) and (13) as $h \triangleq [h_1 \ h_2]$, where $h_1 \triangleq r - \beta e$, $h_2 \triangleq J_\varrho \dot{r} = \chi_\varrho - e - B_\varrho (k_2 r + (k_3 + k_4 \|z_2\|) \operatorname{sgn}(r))$. The closed loop system in (20) has discontinuous signum function, hence the time derivative of (31) exists almost everywhere (a.e.), i.e., for almost all t . Based on [21, Lemma 1], the time derivative of (31), $\dot{V}_\varrho(z_2(t), t) \stackrel{\text{a.e.}}{\in} \dot{V}_\varrho(z_2(t), t)$, where \dot{V}_ϱ is the generalized time derivative of (31) along the Filippov trajectories of $\dot{z}_2 = h(z_2)$ and is defined as in [21] as $\dot{V}_\varrho \triangleq \bigcap_{\xi \in \partial V_\varrho} \xi^T K \begin{bmatrix} \dot{e} & \dot{r} & 1 \end{bmatrix}^T (e, r, t)$. Since $V_\varrho(z_2, t)$ is continuously differentiable in z_2 , $\partial V_\varrho = \{\nabla V_\varrho\}$, thus $\dot{V}_\varrho \stackrel{\text{a.e.}}{\subset} [e \ J_\varrho r \ \frac{1}{2} J_\varrho r^2] K \begin{bmatrix} \dot{e} & J_\varrho \dot{r} & 1 \end{bmatrix}^T$. Therefore, after substituting for (20) and canceling common terms, the generalized time derivative of (31) can be expressed as

$$\begin{aligned} \dot{V}_\varrho \stackrel{\text{a.e.}}{\subset} & -\beta e^2 + r \chi_\varrho \\ & - K[B_\varrho] r [k_2 r + (k_3 + k_4 \|z_2\|) K[\operatorname{sgn}(r)]], \end{aligned} \quad (33)$$

where $K[\operatorname{sgn}(r)] = \operatorname{SGN}(r)$ such that $\operatorname{SGN}(r) = 1$ if $r > 0$; $[-1, 1]$ if $r = 0$; -1 if $r < 0$, and $K[B_\varrho] \subset [\underline{B}_n, \bar{B}_n]$ as

defined in [21]. With the condition in (21) and Property (9), (33) can be upper bounded as

$$\begin{aligned} \dot{\tilde{V}}_{\varrho} \stackrel{a.e.}{\leq} & -\beta e^2 - \underline{B}_n k_2 r^2 + (c_1 - \underline{B}_n k_3) |r| \\ & + (c_2 - \underline{B}_n k_4) |r| \|z_2\|. \end{aligned} \quad (34)$$

Provided the sufficient gain conditions in (30), the following inequality is obtained

$$\tilde{V}_{\varrho} \stackrel{a.e.}{\leq} -\beta e^2 - \underline{B}_n k_2 r^2, \quad (35)$$

$$\stackrel{a.e.}{\leq} -\lambda_{\varrho} \tilde{V}_{\varrho}. \quad (36)$$

Based on (32) and (36), the exponential tracking result in (29) can be obtained. Since $V_{\varrho} \in \mathcal{L}_{\infty}$, $e, r \in \mathcal{L}_{\infty}$ (i.e., $z_2 \in \mathcal{L}_{\infty}$), which implies that $u_{ex}, u_{fl} \in \mathcal{L}_{\infty}$ in (16) and (19). ■

Theorem 3. *A paired motor system has an average dwell time τ_a if there exist positive numbers N_0 and τ_a such that*

$$N(T, t) \leq N_0 + \frac{T-t}{\tau_a}, \quad \forall T \geq t \geq 0, \quad (37)$$

where N is the maximum allowable total switching. The switching motor system ensures exponential tracking with average dwell time [18]

$$\tau_a \geq \frac{\ln(\mu)}{\lambda_{\varrho}}. \quad (38)$$

Proof. Let $t_1, t_2, \dots, t_j, \dots, t_{N_{\sigma}}$ denotes the timing when the motor synchronization controller switched over the time interval $(0, T)$. The switching number for $\varrho = \{ex, fl\}$ motor system over the time interval $(0, T)$ is denoted as $N_{\varrho}(T, t)$, and the total switching number for the whole paired motor system can be written as $N(T, t) = N_{ex}(T, t) + N_{fl}(T, t)$. From the inequality in (32),

$$V_{\varrho}(t_{i+1}) (z_2(t_{i+1})) \leq \mu V_{\varrho}(t_i) (z_2(t_{i+1})), \quad (39)$$

where $\mu = \frac{b_{\varrho}}{a_{\varrho}}$. Define a piecewise differentiable function

$$W(t) = e^{\lambda_{\varrho} t} V_{\varrho}(t) (z_2(t)), \quad (40)$$

which has a non-positive derivative equation

$$\dot{W}(t) = \lambda_{\varrho} W(t) + e^{\lambda_{\varrho} t} \dot{V}_{\varrho}(t) (z_2(t)). \quad (41)$$

Defining t_{i+1}^- the instantaneous time before t_{i+1} , so that the switching system $\varrho(t_{i+1}^-) = \varrho(t_{i+1})$. Considering the time at t_{i+1} with the inequality in (39), non-increasing W in (40) can be expressed as

$$\begin{aligned} W(t_{i+1}) & \leq \exp[\lambda_{\varrho} t_{i+1}] \mu V_{\varrho}(t_i) (z(t_{i+1})) \\ & = \exp[\lambda_{\varrho} t_{i+1}] \mu V_{\varrho}(t_{i+1}^-) (z(t_{i+1})) \\ & = \mu W(t_{i+1}^-) \leq \mu W(t_i). \end{aligned}$$

Applying same method to $W(t_i)$ and the iteration yields the inequality relationship

$$W(T^-) \leq W(t_N) \leq \mu^{N_{\sigma}(T,0)-1} W(0). \quad (42)$$

Substituting (40) into (42) yields

$$\exp[\lambda_{\varrho} T] V_{\varrho}(T^-) (z_2(T)) \leq \mu^{N_{\sigma}(T,0)-1} V_{\varrho}(0) (z_2(0)). \quad (43)$$

After performing algebraic manipulation and substituting the total switching number (37) into the equation yields

$$\begin{aligned} V_{\varrho}(T^-) (z_2(T)) & \leq \\ \exp \left[-\lambda_{\varrho} T + \left(N_0 + \frac{T-t}{\tau_a} - 1 \right) \ln(\mu) \right] & V_{\varrho}(0) (z_2(0)). \end{aligned} \quad (44)$$

The inequality can be further bounded as

$$\begin{aligned} V_{\varrho}(T^-) (z_2(T)) & \leq \exp[(N_0 - 1) \ln(\mu)] \\ \exp \left[\left(\frac{\ln(\mu)}{\tau_a} - \lambda_{\varrho} \right) T \right] & V_{\varrho}(0) (z_2(0)). \end{aligned} \quad (45)$$

Given the condition in (38), $V_{\varrho}(T^-) (z_2(T))$ converges to zero exponentially. ■

V. EXPERIMENTS

An experiment is provided to demonstrate the performance of the controllers developed for kinematic joint tracking in (10) and motor synchronization in (16) and (19) for leg swing. Results from one able-bodied individual (male aged 29 years) were obtained and written informed consent was obtained prior to participation as approved by the Institutional Review Board at Syracuse University. The participant was fitted with the exoskeleton, and instructed to keep the right leg standing while avoiding providing voluntary effort on the left leg.

The customized exoskeleton was designed for fitting a wide variety of body sizes and maintaining alignment with the user's joints. There were 2 brushless 24 VDC electric motors (Maxon) used to actuate the cable-driven mechanisms. The angles of motor and joint were measured by Maxon motor's encoders and a optical encoder (US Digital), respectively. The controllers were implemented on a desktop computer (Windows 10 OS) running a real-time target (QUARC 2.6, Quanser) via MATLAB/Simulink 2018a (MathWorks Inc) with a sample rate of 1 kHz. A Quanser QPIDE and a Q-8 DAQ boards were used to read the encoders, and control the servo motor drivers (Maxon) operating in current-controlled mode.

Figure 2 illustrates the exoskeleton testbed. The safety precautions include: an emergency stop button was installed near the user to stop the experiment manually, software stop conditions to ensure the testbed was performing in safe range of motion, and mechanical stops were designed on exoskeleton to avoid moving the legs through unsafe joint angles. The desired left knee trajectory was designed to vary from 10 deg to 80 deg with a period of 3 seconds. The control gains introduced in (10), (16) and (19) were selected as follows: $k_1 = 2, \epsilon = 2, \alpha = 10, k_2 = 0.01, k_3 = 0.2, k_4 = 0.0001, \beta = 30$. The experiment was implemented for a duration of 60 seconds. Figure 3 shows the desired and actual joint angles. The exoskeleton control input is presented in

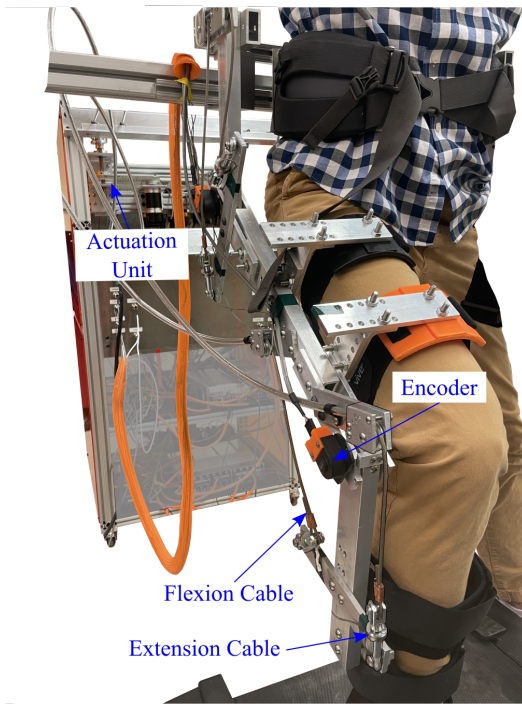


Fig. 2. Cable-driven exoskeleton testbed used for experiment demonstration. The system uses flexion and extension cables to apply torque at each joint using electrical motors installed in the actuation unit.

Figure 4. Figure 5 illustrates the performance of the synchronization tracking objective. The applied synchronization motor control inputs are depicted in Figure 6.

VI. CONCLUSION

The dynamical model for a human-exoskeleton and motor systems were introduced. A high-gain exoskeleton controller and a motor synchronization controller with sliding-mode method were developed. A Lyapunov-based stability analysis is developed to ensure globally ultimately bounded for the joint tracking objective, and exponential tracking for the motor synchronization objective. The average dwell time condition provides a bound on the number of motor switches and guarantees exponential tracking for the switching motors. Future work includes developing a force controller to improve tracking performance, and evaluate the control performance in walking experiments.

REFERENCES

- [1] A. Rodríguez-Fernández, J. Lobo-Prat, and J. M. Font-Llagunes, "Systematic review on wearable lower-limb exoskeletons for gait training in neuromuscular impairments," *Journal of NeuroEngineering and Rehabilitation*, vol. 18, no. 1, pp. 1–22, 2021.
- [2] S. R. Chang, M. J. Nandor, L. Li, *et al.*, "A muscle-driven approach to restore stepping with an exoskeleton for individuals with paraplegia," *Journal of NeuroEngineering and Rehabilitation*, vol. 14, no. 1, pp. 1–12, 2017.
- [3] K. A. Shorter, G. F. Kogler, E. Loth, *et al.*, "A portable powered ankle-foot orthosis for rehabilitation," *Journal of Rehabilitation Research and Development*, vol. 48, no. 4, pp. 459–472, 2011.

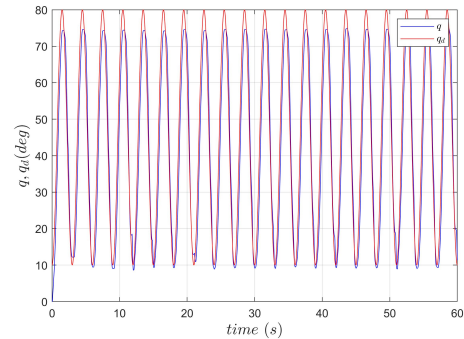


Fig. 3. Joint angle trajectory tracking performance depicting the joint desired trajectory q_d and actual joint trajectory q .

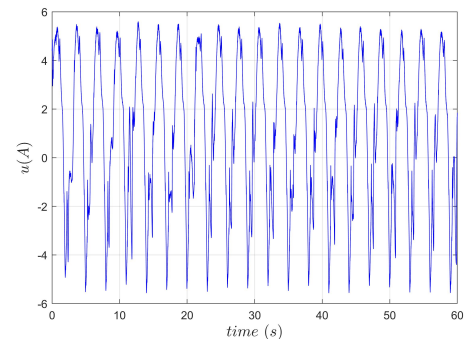


Fig. 4. Control input u for joint tracking.

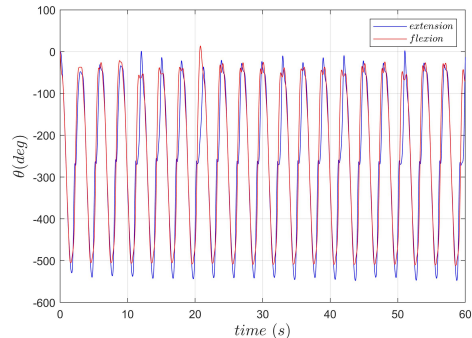


Fig. 5. Motor synchronization trajectory tracking illustrating the motor flexion angle θ_{fl} and motor extension angle θ_{ex} .

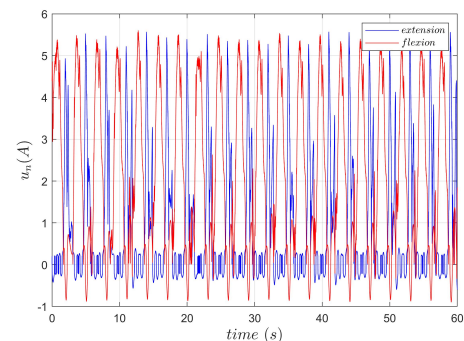


Fig. 6. Synchronization control input for flexor u_{fl} and extensor u_{ex} .

- [4] R. Chin, E. T. Hsiao-Wecksler, E. Loth, *et al.*, “A pneumatic power harvesting ankle-foot orthosis to prevent foot-drop,” *Journal of NeuroEngineering and Rehabilitation*, vol. 6, no. 1, pp. 1–11, 2009.
- [5] J. D. Sanjuan, A. D. Castillo, M. A. Padilla, *et al.*, “Cable driven exoskeleton for upper-limb rehabilitation: A design review,” *Robotics and Autonomous Systems*, vol. 126, 2020.
- [6] G. Lv, H. Zhu, and R. D. Gregg, “On the design and control of highly backdrivable lower-limb exoskeletons,” *IEEE Control Sys.*, vol. 28, no. 6, pp. 88–113, 2018.
- [7] G. M. Bryan, P. W. Franks, S. C. Klein, *et al.*, “A hip–knee–ankle exoskeleton emulator for studying gait assistance,” *International Journal of Robotics Research*, 2020.
- [8] A. T. Asbeck, K. Schmidt, I. Galiana, *et al.*, “Multi-joint soft exosuit for gait assistance,” *Proceedings - IEEE International Conference on Robotics and Automation*, vol. 2015-June, no. June, pp. 6197–6204, 2015.
- [9] T. Noda, T. Teramae, B. Ugurlu, *et al.*, “Development of an upper limb exoskeleton powered via pneumatic electric hybrid actuators with bowden cable,” *IEEE International Conference on Intelligent Robots and Systems*, no. Iros, pp. 3573–3578, 2014.
- [10] T. Lenzi, N. Vitiello, S. M. M. De Rossi, *et al.*, “NEUROExos: A variable impedance powered elbow exoskeleton,” *Proceedings - IEEE International Conference on Robotics and Automation*, pp. 1419–1426, 2011.
- [11] A. Chiri, F. Giovacchini, N. Vitiello, *et al.*, “HANDEXOS: Towards an exoskeleton device for the rehabilitation of the hand,” *2009 IEEE/RSJ International Conference on Intelligent Robots and Systems, IROS 2009*, pp. 1106–1111, 2009.
- [12] R. Verhoeven, “Analysis of the Workspace of Tendon-Based,” *Duisburg Gerhard Mercator University*, 2003.
- [13] H. Wu, M. Yin, Z. Xu, *et al.*, “Transmission Characteristics Analysis and Compensation Control of Double Tendon-sheath Driven Manipulator,” *Sensors*, vol. 20, no. 5, p. 1301, 2020.
- [14] B. Okur, O. Aksoy, E. Zergeroglu, *et al.*, “Nonlinear Robust Control of Tendon-Driven Robot Manipulators,” *Journal of Intelligent and Robotic Systems: Theory and Applications*, vol. 80, no. 1, pp. 3–14, 2015.
- [15] H. Lu, X. Zhang, and X. Huang, “Robust Adaptive Control of Antagonistic Tendon-Driven Joint in the Presence of Parameter Uncertainties and External Disturbances,” *Journal of Dynamic Systems, Measurement and Control, Transactions of the ASME*, vol. 139, no. 10, pp. 1–10, 2017.
- [16] W. Ouyang, H. Chi, J. Pang, *et al.*, “Adaptive Locomotion Control of a Hexapod Robot via Bio-Inspired Learning,” *Frontiers in Neurobotics*, vol. 15, no. January, 2021.
- [17] Y. Mao and S. K. Agrawal, “A cable driven upper arm exoskeleton for upper extremity rehabilitation,” *Proceedings - IEEE International Conference on Robotics and Automation*, pp. 4163–4168, 2011.
- [18] D. Liberzon, *Switching in systems and control*. Birkhauser, 2003.
- [19] F. L. Lewis, D. M. Dawson, and C. T. Abdallah, *Robot Manipulator Control Theory and Practice*. Marcel Dekker, 2003.
- [20] B. E. Paden and S. S. Sastry, “A Calculus for Computing Filippov’s Differential Inclusion with Application to the Variable Structure Control of Robot Manipulators,” *IEEE Transactions on Circuits and Systems*, vol. 34, no. 1, pp. 73–82, 1987.
- [21] N. Fischer, R. Kamalapurkar, and W. E. Dixon, “LaSalle-Yoshizawa corollaries for nonsmooth systems,” *IEEE Transactions on Automatic Control*, vol. 58, no. 9, pp. 2333–2338, 2013.